Materials Research Letters

ISSN: (Print) (Online) Journal homepage: https://www.tandfonline.com/loi/tmrl20

Superior strength-ductility synergy by hetero-structuring high manganese steel

Xing Fang , Qiqi Xue , Kaiyuan Yu , Runguang Li , Daqiang Jiang , Lei Ge , Yang Ren , Changfeng Chen & Xiaolei Wu

To cite this article: Xing Fang , Qiqi Xue , Kaiyuan Yu , Runguang Li , Daqiang Jiang , Lei Ge , Yang Ren , Changfeng Chen & Xiaolei Wu (2020) Superior strength-ductility synergy by hetero-structuring high manganese steel, Materials Research Letters, 8:11, 417-423, DOI: 10.1080/21663831.2020.1780330

To link to this article: https://doi.org/10.1080/21663831.2020.1780330

© 2020 The Author(s). Published by Informa UK Limited, trading as Taylor & Francis Group

Published online: 01 Jul 2020.

Submit your article to this journal

Article views: 594

View related articles

View Crossmark data

Full Terms & Conditions of access and use can be found at
https://www.tandfonline.com/action/journalInformation?journalCode=tmrl20

MATER. RES. LETT.
2020, VOL. 8, NO. 11, 417–423
https://doi.org/10.1080/21663831.2020.1780330

MATERIALS RESEARCH LETTERS
Taylor & Francis
Taylor & Francis Group

ORIGINAL REPORT

OPEN ACCESS Check for updates

Superior strength-ductility synergy by hetero-structuring high manganese steel

Xing Fang[a]*, Qiqi Xue[b,c]*, Kaiyuan Yu[a], Runguang Li [d], Daqiang Jiang[a], Lei Ge[a], Yang Ren[e], Changfeng Chen[a] and Xiaolei Wu[b,c]

[a]Department of Materials Science and Engineering, China University of Petroleum-Beijing, Beijing, People's Republic of China; [b]State Key Laboratory of Nonlinear Mechanics, Institute of Mechanics, Chinese Academy of Sciences, Beijing, People's Republic of China; [c]School of Engineering Science, University of Chinese Academy of Sciences, Beijing, People's Republic of China; [d]State Key Laboratory for Advanced Metals and Materials, University of Science and Technology Beijing, Beijing, People's Republic of China; [e]X-ray Science Division, Advanced Photon Source, Argonne National Laboratory, IL, USA

ABSTRACT

Lacking of forest hardening makes low ductility in steels long challenge particularly at high yield strength. Here, we report to make good use of hetero-structuring for superior strength-ductility synergy in high manganese steel. The point is to retain original deformed structure of large quantity, along with recrystallized ultrafine-grains and fine grains, jointly for most effective heterogeneous deformation-induced (HDI) hardening especially at high strength. The residual plastic strain of larger than 0.2% and large proportion of HDI stress over 60% indicate the crucial role in ductility by HDI hardening. This renders a significantly upgraded strength-ductility combination within high strength scope.

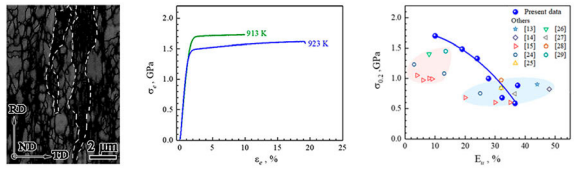

IMPACT STATEMENT

By using the hetero-structuring strategy, a superior strength-ductility synergy is realized specifically at ultra-high strength in high manganese steel.

ARTICLE HISTORY
Received 31 March 2020

KEYWORDS
Hetero-structuring; heterogeneous deformation-induced strain hardening; ductility; ultra-high strength steel; high manganese steel

In advanced high strength steels for structural applications, to pursue the superior $(\sigma_y, \varepsilon_u)$ combination causes long concern [1–8], where σ_y is the yield strength and ε_u is the tensile uniform strain. So far, the real challenge lies in low ε_u particularly at high and even ultra-high σ_y [1–3], typical of the $(\sigma_y, \varepsilon_u)$ trade-off. The crux of the problem is inadequate strain hardening, which can no longer keep up with high flow stress to circumvent plastic instability [6–8], i.e. necking via strain localization, as predicted by the Considerè criterion. On one hand, high σ_y is usually obtained by either cold work or plastic deformation-induced grain refinement. However, such strengthening comes at the expense of strain hardening [6–8], because intra-granular dislocation plasticity, a potent mechanism for strain hardening, almost disappears. On the other hand, several other strategies for strain hardening take effect mainly at low σ_y in coarse-grained structures, including the transformation-induced plasticity (TRIP) effect [1,5,9], twinning-induced plasticity effect [10,11], second phase [4], and nano-precipitates [3] etc. Even austenite, as ductile phase in steels, is no exception. For example, ε_u almost disappears at σ_y of 1.45 GPa in 316L austenite stainless steel [12]. The high manganese steel of usually with Mn content larger than 10 wt% [13–15], along with recently well-developed medium-Mn (6–10 wt%) steels

CONTACT Kaiyuan Yu kyyu@cup.edu.cn Department of Materials Science and Engineering, China University of Petroleum-Beijing, Changping, Beijing 102249, People's Republic of China; Xiaolei Wu xlwu@imech.ac.cn School of Engineering Science, University of Chinese Academy of Sciences, Beijing 100190, People's Republic of China
*These authors contributed equally to this work.

Supplemental data for this article can be accessed here. https://doi.org/10.1080/21663831.2020.1780330

© 2020 The Author(s). Published by Informa UK Limited, trading as Taylor & Francis Group
This is an Open Access article distributed under the terms of the Creative Commons Attribution License (http://creativecommons.org/licenses/by/4.0/), which permits unrestricted use, distribution, and reproduction in any medium, provided the original work is properly cited.

[1,16], features the TRIP effect for large ε_u. However, the TRIP effect will be out of operation at high σ_y. A few exceptions occur in medium-Mn steels due to special carbon partitioning [1], which is, however, not applicable to high-Mn steels.

Recently, the hetero-structure (HS) of varying kinds arouses an ongoing interest for distinct heterogeneous deformation-induced (HDI) hardening [17–20], which is particularly effective to elevate ε_u at high σ_y [19,20]. Several typical HSs demonstrate the key role by HDI hardening, including hetero-lamellar structure [19] and three-level grain heterogeneity [20]. The pre-requisite for HDI hardening is microstructural heterogeneities of contrasting mechanical responses upon straining [17,18]. Here we take the HS strategy one step further by pushing for a highly heterogeneous microstructure. The core idea is to reserve the deformed structure as much as possible for high σ_y, while only fewer recrystallized grains for effective HDI hardening. This tailored HS thus shows an extraordinary HDI hardening, providing perfectly acceptable ε_u of 10% at σ_y of 1.7 GPa, along with an upgrade $(\sigma_y, \varepsilon_u)$ synergy.

The high-Mn steel is a good model to work with, having face-centered-cubic structured single-phase austenite. The chemical composition was Fe-16Mn-0.5C, weight percent. The starting bar ingot was cast through vacuum smelting, which was hot-forged and then hot-drawn into wires of 0.67 mm in diameter, followed by solution treatment at 1423 K for 2 h and water cooling. The wire was then cold-drawn to 0.33 mm in diameter followed by recrystallization annealing at various temperatures for 10 min. Tensile testing was carried out at strain rate of 1×10^{-3} s^{-1} at room temperature. The gauge length of the tensile samples was 50 mm. The extenso-meter was used for strain measurement. Microstructural characterization was conducted by using ZEISS Supra 55 scanning electron microscope (SEM) with electron backscatter diffraction (EBSD) detector and FEI Tecnai G2 F20 TEM. TEM specimens were prepared by mechanical grinding, polishing and low energy ion milling. The synchrotron-based high energy XRD *in situ* experiments were performed at Advanced Photon Source (APS), Argonne National Laboratory, USA. Refer to Ref. [21] for the experimental details.

Figure 1(a) is the EBSD quality image showing the HS after annealing at 923 K. The HS consists of the fiber-like deformed structure (outlined by dotted line in white) and crystallized equiaxed grains. TEM images show elongated structure of tangled dislocations, see Figure 1(b), and crystallized grains, see Figure 1(c), respectively. Both insets are selected area electron diffraction (SAED) patterns, indicating face-centered cubic structured γ-austenite. This is in line with XRD spectrum tested before and after tensile testing, see Figure 1(f). The single-phase γ-austenite exists, without detectable either hcp or bcc phase. Figure 1(d) is TEM image showing another HS after annealing at 913 K. The similar microstructural feature is visible to that at 923 K. Figure 1(e) shows size distribution of recrystallized grains in HS after annealing at 923 K based on statistic data of several hundreds of grains from EBSD and TEM images. Inset is the distribution of aspect ratio of long to short axis, α. Obviously, the HS is trans-scale, with grain sizes spanning UFG to FG. The UFG has an average grain size $\bar{d}_{UFG}$, of 0.34 μm, number density ρ_{UFG} (number/μm^2) of 92.2%, and volume fraction f_{vol} of 67%. The corresponding data for FG is, respectively, ~1.2 μm, 7.8%, and ~33%. The mean aspect ratio is 1.37, much larger than 1. Moreover, the volume fraction of recrystallized grains is 48.3% and 17.5%, respectively, in HS after annealing at 923 and 913 K. This indicates that the HS is in a severely deformed state, with a mass of deformed structure preserved.

Figure 2(a) shows two tensile engineering stress–strain $(\sigma_e - \varepsilon_e)$ curves. σ_y is 1450 MPa and ε_u is 20% after annealing at 923 K. σ_y increases to 1700 MPa, ε_u still keeps 10% at annealing temperature at 913 K. Continuous yielding appears, which differs from yield-drop followed by an extended Lüders plateau in nearly all medium-Mn steels at elevated σ_y [1,16]. All $(\sigma_e - \varepsilon_e)$ curves at varying annealing temperatures are shown in Fig. S1 in Supplementary. Figure 2(b,c) are, respectively, true stress–strain $(\sigma_{true} - \varepsilon_{true})$ curves and strain hardening rate $(\vartheta = \partial\sigma/\partial\varepsilon)$-$\varepsilon_{true}$ curves. Interestingly, an upturn of ϑ appears during the early stage of small strains in sample after annealing at 923 K. The upturn of ϑ is widely observed in varying microstructures with varying deformation physics [14,19,22,23]. The trans-scale HS facilitates a largely extended elasto-plastic transition when HDI hardening already works. This is probably the reason of upturn in ϑ [19,22]. Figure 2(d) shows the $(\sigma_y, \varepsilon_u)$ combination of all HSs. The data are also summarized of other high-Mn steels for comparison [13–15,24–29]. Two areas are distinguishable of high and low σ_y. Our data stand out with enhanced ε_u within the range of high σ_y, leading to upgraded $(\sigma_y, \varepsilon_u)$ synergy. This is indicative of special advantage of the present HS for strain hardening.

The interrupted unload-reload tensile tests were conducted to reveal strain hardening, see Figure 3(a). The hysteresis loops recur during each unloading-reloading cycle. This signals the Bauschinger effect. The loop width is characterized by residual plastic strain, ε_{rp}, following elastic unload, see Figure 3(b). Of special note is record-wide loops. ε_{rp} is even larger than 0.2% starting from unload strain of 5%, see Figure 3(c). This indicates that the compressive plastic flow sets in already upon elastic unload, even though applied stress is still under

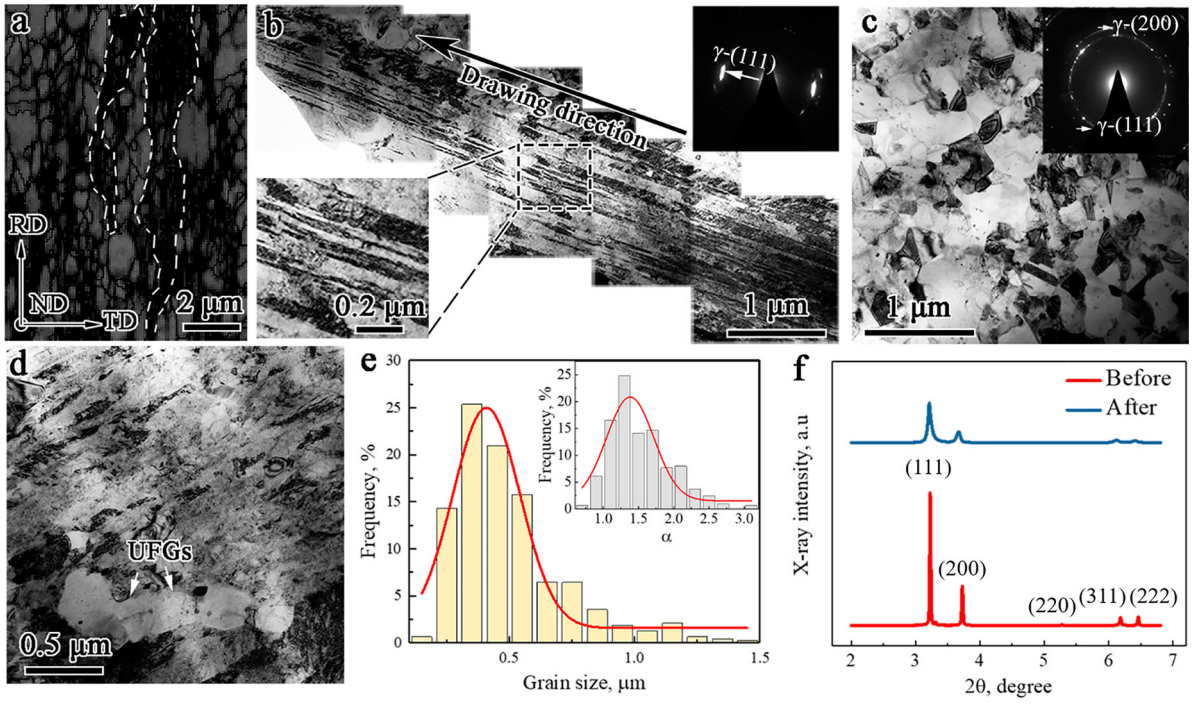

Figure 1. Heterogeneous structure (HS). All for HS after annealing at 923 K except for (c) at 913 K. (a) EBSD quality image. A few areas encircled by dotted line are fiber-like deformed structure. (b), (c), and (d) TEM images showing elongated lamellae and recrystallized grains. Insets in (b) and (c) are SAED pattern. (e) Statistic grain size distribution and aspect ratio (inset) for recrystallized grains. (f) XRD spectrum before and after tensile testing.

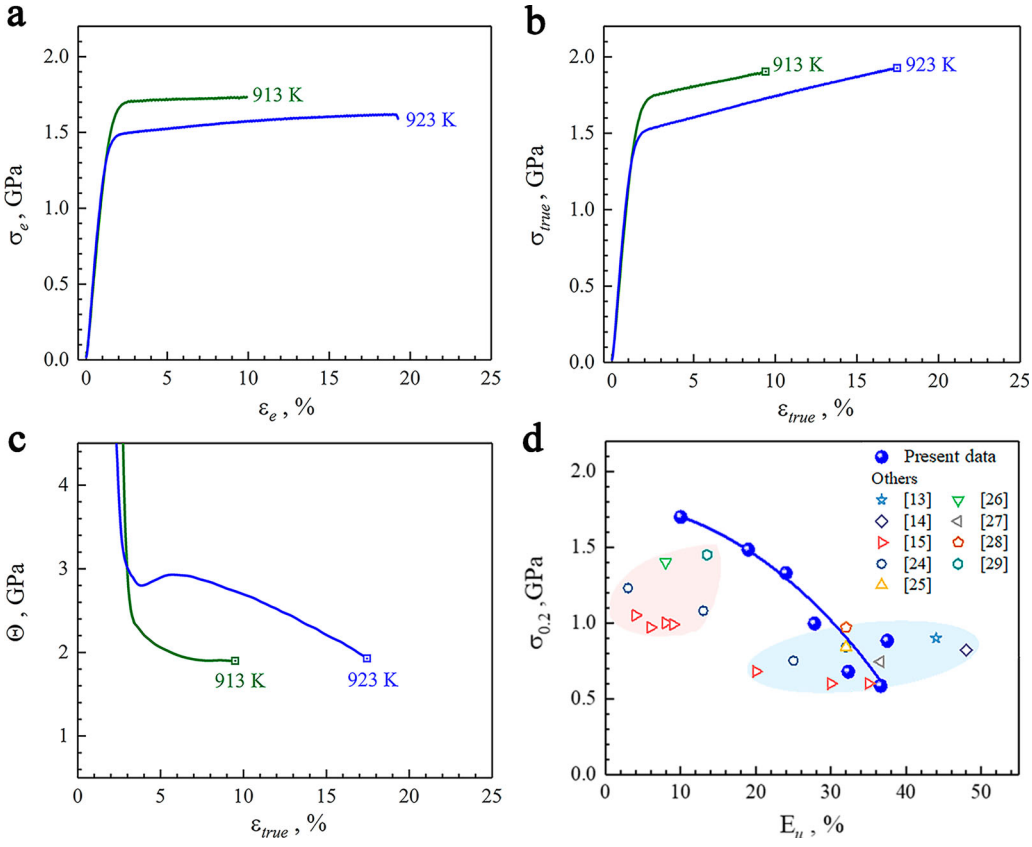

Figure 2. Tensile property. (a) $\sigma_e - \varepsilon_e$ curves after annealing at 913 and 923 K. (b) $\sigma_{true} - \varepsilon_{true}$ curves. (c) ϑ-ε_{true} curves. (d) (σ_y,ε_u) synergy.

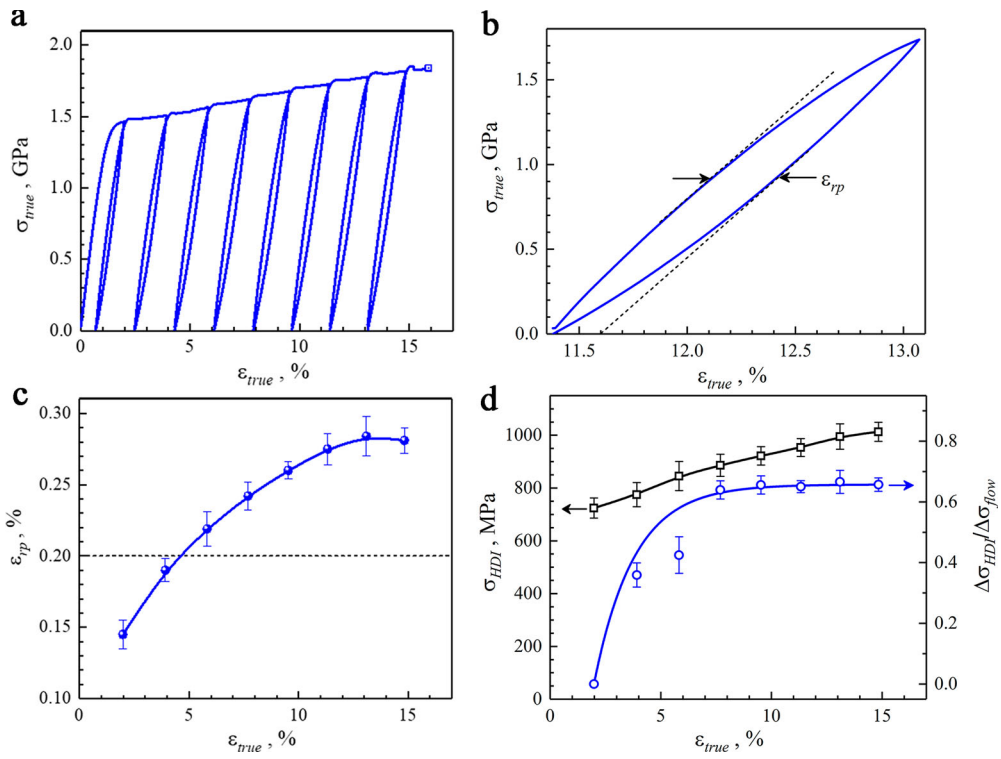

Figure 3. HDI stress. (a) Tensile $\sigma_{true} - \varepsilon_{true}$ curve. (b) Hysteresis loop at unload strain of 13%. (c) ε_{rp} versus ε_{true} curve. (d) $\Delta\sigma_{\mathrm{HDI}}$ and $\Delta\sigma_{HDI}/\Delta\sigma_{flow}$ versus ε_{true} curve.

tension. This is an unambiguous sign which unequivocally demonstrates the key effect of back stress, as a part of HDI stress (σ_{HDI}) [19,30,31]. Further, both the heterogeneous deformation-induced (HDI) stress, σ_{HDI}, together with the proportion, λ, of $\Delta\sigma_{\mathrm{HDI}}$ to $\Delta\sigma_{\mathrm{flow}}$ were calculated, see Figure 3(d), where $\Delta\sigma_{\mathrm{HDI}}$ and $\Delta\sigma_{\mathrm{flow}}$ are the increment of both σ_{HDI} and σ_{flow} after yielding, respectively, by subtracting σ_{HDI} and σ_{flow} at offset strain of 0.2%. Refer to Ref. [30] for the method of calculating $\Delta\sigma_{\mathrm{HDI}}$. It is visible that σ_{HDI} increases with tensile strain. At the same time, λ rises rapidly to 65% at first and then levels off. The trend of both σ_{HDI} and λ is well in line with that in other HSs [19,20], indicating the crucial role by HDI hardening throughout tensile deformation.

The microscopic plastic response was further investigated by using synchrotron-based high energy *in situ* XRD tensile load, see Figure 4(a). The change of axial lattice strain with applied stress is shown in Figure 4(b). The equation for lattice strain calculation is given in Supplementary. Interestingly, lattice strain of (111) grain family begins to deviate from linearity at stress of 1150 MPa, in contrast to macroscopic σ_y of 1450 MPa. This is micro-yielding which happens at first in (111) grain family. This indicates an extended elasto-plastic transition, inherent to the trans-scale HS [19,20]. After global yielding, the rate of increase in lattice strain speeds up in (200) and (311) grain family, tilting linear lattice strain to the right. (200) grain family comes fastest, (311) second, in sharp contrast to the trend in (111) and (220) families. This indicates load partitioning during tensile deformation. Namely, (111) and (220) grain families carry less loads, whilst (200) and (311) will bear a proportionally increasing fraction of applied loads. The load partitioning is, actually, the direct result of HDI stress [19,20]. Moreover, the dislocation density, ρ, is measured according to the modified Williamson-Hall (W-H) equation [32], see Supplementary for the calculation method. ρ shows an initial rapid rise and then level-off during tensile deformation, see Figure 4(c).

Finally, TEM observations show that the deformation nanotwins (Figure 5(a)), stacking faults (Figure 5(b)), and tangled high-density dislocations (Figure 5(c)) are all formed inside recrystallized grains during tensile deformation.

The present HS consists of the deformed structure in large amounts, together with recrystallized UFGs and FGs. Therein, contrasting plastic responses of two kinds are seen. One is σ_y, from big to small in the order of the deformed structure, UFGs, and FGs. This is the reason for micro-yielding, which happens at first in (111) grain family at 1150 MPa, $\sim$300 MPa below global σ_y. The other is strain hardening, which is almost absent in deformed structure, limited in UFGs [6,7], while extraordinary in FGs. This induces the polarization of strain

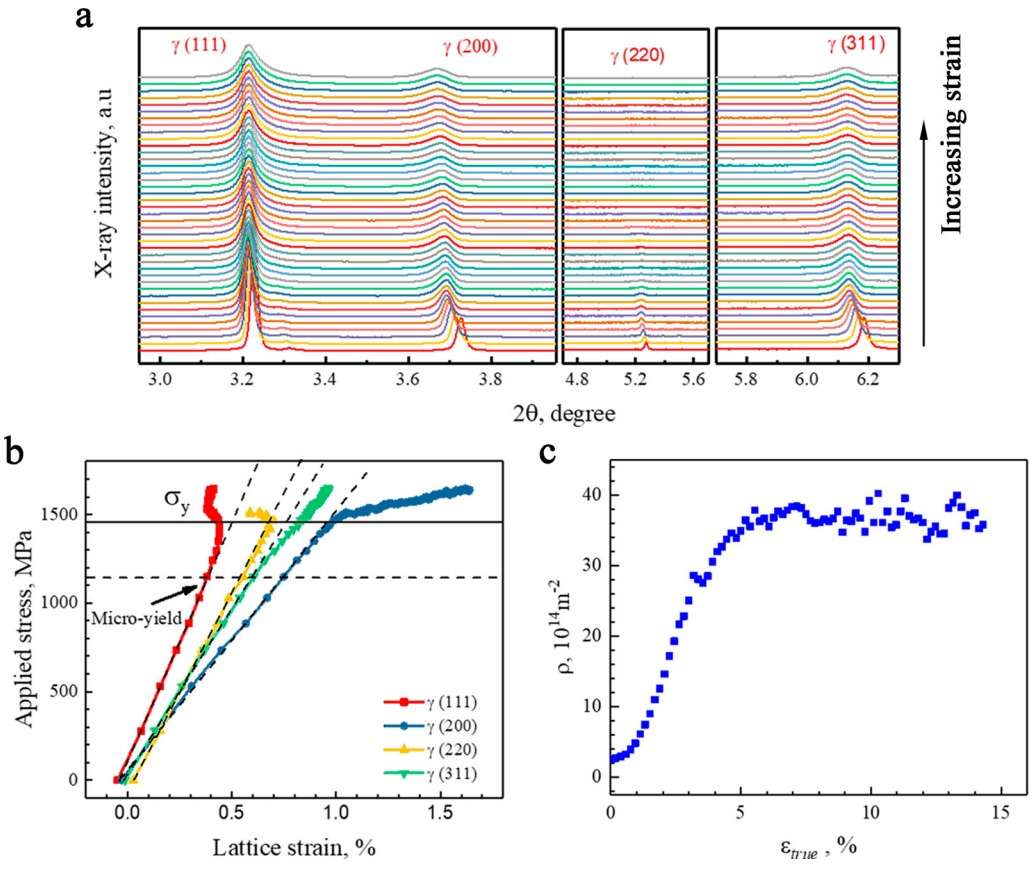

Figure 4. Synchrotron-based *in situ* XRD tensile loading. (a) XRD spectrum in varying crystal planes. (b) Applied stress *vs* lattice strain curves. Arrow indicates the onset of micro-yield in (111) grain family. (c) ρ *vs* ε_{true} curve.

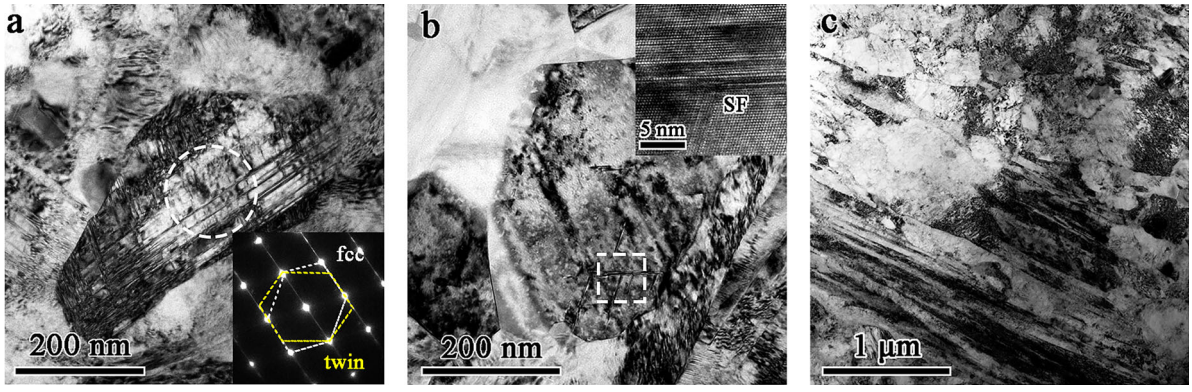

Figure 5. TEM observations of microstructural evolution. (a) Deformation twins. Inset: SAED pattern showing twin relationship. (b) Stacking faults (SFs). Inset: high-resolution TEM image showing lattice image of SF. (c) Tangled dislocations of high density.

localization versus plastic stability. As a result, tensile deformation is highly heterogeneous inside the HS. This causes a local, additional stress, defined as HDI stress [18], at hetero-interfaces between grains of contrasting plastic responses. The HDI stress is a pair of balancing forces: back stress imposed on ductile FGs and opposite forward stress on the strong deformed structure. The dislocation model of back stress is proposed for strain hardening in terms of the pile-up of geometrically necessary dislocations (GNDs) [18,33–36]. Correspondingly, HDI hardening is experimentally evidenced later [18], serving as a combined effect induced by back stress and forward stress [37].

The HDI hardening is dominant in the present HS. It is worthy to note the initial rise followed by level-off for both λ (Figure 3(d)) and ρ (Figure 4(c)) as tensile strain increases, in contrast to the monotonic rise in both ε_{rp} (Figure 3(c)) and σ_{HDI} (Figure 3(d)). The initial rise in ρ is due to the storage of dislocations into FGs, while that for the remaining is ascribed to the onset of HDI

hardening as early as micro-yielding. With further straining, the rise of both σ_{HDI} and ε_{rp} indicates that HDI hardening continues to play a key role during tensile deformation. At this stage, the dislocation cross slip happens such that both the generation and annihilation of dislocations co-exist, typical of Stage III of strain hardening [38]. This is the reason of level-off in ρ. It is further argued that the softening effect emerges in deformed structure and even UFGs due to forward stress. Namely, forest hardening weakens gradually. Therefore, the percentage of σ_{HDI} (Figure 3(d)), as a comprehensive effect of strain hardening by back stress and softening, levels off. In other words, HDI hardening plays an increasing role throughout tensile deformation, in line with growing σ_{HDI}. In addition, HDI hardening is in action already during micro-yielding, which leads to strengthening to increase σ_y [19,20,31].

FGs plays a key role in strain hardening by back stress in the present HS. Specifically, the smaller grain size within the micron-scale regime, the stronger effect of dislocation pile-up for strain hardening [35,36], and hence, the stronger HDI hardening will be. Therefore, FGs of $\bar{d}$ of 1.2 μm play a significant role in ductility. Reasonably, the less volume fraction of FGs, the weaker HDI hardening will be. This is probably the reason of less uniform strain in HS after annealing at 913 K than that at 923 K. Yet, yield strength increases by 250 MPa.

In summary, the hetero-structuring strategy is applied to an old high-Mn steel for ductility at high yield strength. The HDI hardening plays a dominant role in ductility. The present study helps out for understanding deformation physics in the HS for tailoring the microstructure to upgrade the strength and ductility combination.

Disclosure statement

No potential conflict of interest was reported by the author(s).

Funding

Financial supports were acknowledged from NSFC [grant numbers 51871241, 91963112, and 11972350], MOST [grant number 2017YFA0204402], and CAS [grant number XDB2204 0503]. The use of the Advanced Photon Source was supported by the US Department of Energy, Office of Science, and Office of Basic Energy Science under Contract No. DE-AC02-06CH11357.

ORCID

Runguang Li http://orcid.org/0000-0001-5395-0470

References

[1] He BB, Hu B, Yen HW, et al. High dislocation density-induced large ductility in deformed and partitioned steels. Science. 2017;357:1029–1032.
[2] Liu L, Yu Q, Wang Z, et al. Making ultrastrong steel tough by grain-boundary delamination. Science. 2020. doi:10.1126/science.aba9413.
[3] Jiang SH, Wang H, Wu Y, et al. Ultrastrong steel via minimal lattice misfit and high-density nanoprecipitation. Nature. 2017;544:460–464.
[4] Kim SH, Kim H, Kim NJ. Brittle intermetallic compound makes ultrastrong low-density steel with large ductility. Nature. 2015;518:77–79.
[5] Herrera C, Ponge D, Raabe D. Design of a novel Mn-based 1 GPa duplex stainless TRIP steel with 60% ductility by a reduction of austenite stability. Acta Mater. 2011;59:4653–4664.
[6] Zhu YT, Liao XZ. Nanostructured metals: retaining ductility. Nat Mater. 2004;3:351–352.
[7] Ovid'ko IA, Valiev RZ, Zhu YT. Review on superior strength and enhanced ductility of metallic nanomaterials. Prog Mater Sci. 2018;94:462–540.
[8] Ma E, Wu XL. Tailoring heterogeneities in high-entropy alloys to promote strength–ductility synergy. Nat Commun. 2019;10:5623.
[9] Wu XL, Yang MX, Yuan FP, et al. Combining gradient structure and TRIP effect to produce austenite stainless steel with high strength and ductility. Acta Mater. 2016;112:337–346.
[10] Bouaziz O, Guelton N. Modelling of TWIP effect on work-hardening. Mater Sci Eng A. 2001;319–321:246–249.
[11] Gutierrez-Urrutia I, Raabe D. Grain size effect on strain hardening in twinning-induced plasticity steels. Scr Mater. 2012;66:992–996.
[12] Chen XH, Lu J, Lu L, et al. Tensile properties of a nanocrystalline 316L austenitic stainless steel. Scr Mater. 2005;52:1039–1044.
[13] Koyama M, Lee T, Lee CS, et al. Grain refinement effect on cryogenic tensile ductility in a Fe-Mn-C twinning-induced plasticity steel. Mater Des. 2013;49:234–241.
[14] Tian YZ, Bai Y, Zhao LJ, et al. A novel ultrafine-grained Fe–22Mn–0.6C TWIP steel with superior strength and ductility. Mater Charact. 2017;126:74–80.
[15] Dini G, Najafizadeh A, Ueji R, et al. Improved tensile properties of partially recrystallized submicron grained TWIP steel. Mater Lett. 2010;64:15–18.
[16] Hu B, Luo HW, Yang F, et al. Recent progress in medium-Mn steels made with new designing strategies, a review. J Mater Sci Technol. 2017;33:1457–1464.
[17] Wu XL, Zhu YT. Heterogeneous materials: a new class of materials with unprecedented mechanical properties. Mater Res Lett. 2017;5:527–532.
[18] Zhu YT, Wu XL. Perspective on hetero-deformation induced (HDI) hardening and back stress. Mater Res Lett. 2019;7:393–398.
[19] Wu XL, Yang MX, Yuan FP, et al. Heterogeneous lamella structure unites ultrafine-grain strength with coarse-grain ductility. Proc Natl Acad Sci. 2015;112:14501–14505.
[20] Yang MX, Yan DS, Yuan FP, et al. Dynamically reinforced heterogeneous grain structure prolongs ductility in a medium-entropy alloy with gigapascal yield strength. Proc Natl Acad Sci. 2018;115:7224–7229.

[21] Jia N, Cong ZH, Sun X, et al. An in situ high-energy X-ray diffraction study of micromechanical behavior of multiple phases in advanced high-strength steels. Acta Mater. 2009;57:3965–3977.
[22] Wu XL, Jiang P, Chen L, et al. Extraordinary strain hardening by gradient structure. Proc Natl Acad Sci. 2014;111:7197–7201.
[23] Tian YZ, Zhao LJ, Park N, et al. Revealing the deformation mechanisms of Cu–Al alloys with high strength and good ductility. Acta Mater. 2016;110:61–72.
[24] Lu K, Yan FK, Wang HT, et al. Strengthening austenitic Fe-Mn steels by using nanotwinned austenitic grains. Acta Mater Mater. 2012;66:878–883.
[25] Lee T, Koyama M, Tsuzaki K, et al. Tensile deformation behavior of Fe-Mn-C TWIP steel with ultrafine elongated grain structure. Mater Lett. 2012;75:169–171.
[26] Bouaziz O, Scott CP, Petitgand G. Nanostructured steel with high work-hardening by the exploitation of the thermal stability of mechanically induced twins. Scr Mater. 2009;60:714–716.
[27] Li Y, Lu YF, Li W, et al. Hierarchical microstructure design of a bimodal grained twinning-induced plasticity steel with excellent cryogenic mechanical properties. Acta Mater. 2018;158:79–94.
[28] Behjati P, Kermanpur A, Najafizadeh A, et al. Enhanced mechanical properties in a high-manganese austenitic steel through formation of nano grains, nanotwinned austenite grains, nano carbides and TRIP. Mater Sci Eng A. 2014;610:273–278.
[29] Zhou P, Liang ZY, Liu RD, et al. Evolution of dislocations and twins in a strong and ductile nanotwinned steel. Acta Mater. 2016;111:96–107.
[30] Yang MX, Pan Y, Yuan FP, et al. Back stress strengthening and strain hardening in gradient structure. Mater Res Lett. 2016;4:145–151.
[31] Wu XL, Jiang P, Chen L, et al. Synergetic strengthening by gradient structure. Mater Res Lett. 2014;2:185–191.
[32] Zhang MH, Li RG, Ding J, et al. In situ high-energy X-ray diffraction mapping of Lüders band propagation in medium-Mn transformation-induced plasticity steels. Mater Res Lett. 2018;6:662–667.
[33] Ashby MF. The deformation of plastically non-homogeneous materials. Philos Mag. 1970;21:399–424.
[34] Nix WD, Gao HJ. Indentation size effects in crystalline materials: A law for strain gradient plasticity. J Mech Phys Solids. 1998;46:411–425.
[35] Wei YG, Wang XZ, Wu XL, et al. Theoretical and experimental researches of size effect in micro-indentation test. Sci China Ser A Math. 2001;44:74–82.
[36] Xiang Y, Vlassak JJ. Bauschinger and size effects in thin-film plasticity. Acta Mater. 2006;54:5449–5460.
[37] Yuan FP, Yan DS, Sun JD, et al. Ductility by shear band delocalization in the nano-layer of gradient structure. Mater Res Lett. 2019;7:12–17.
[38] Kocks UF, Mecking H. Physics and phenomenology of strain hardening: the FCC case. Prog Mater Sci. 2003;48:171–273.